Gemini and *Hubble Space Telescope* Evidence for an Intermediate Mass Black Hole in omega Centauri

Eva Noyola and Karl Gebhardt

Astronomy Department, University of Texas at Austin, Austin, TX 78712

`noyola@mpe.mpg.de`

Marcel Bergmann

Gemini Observatory, Tucson, AZ 85726

ABSTRACT

The globular cluster ω Centauri is one of the largest and most massive members of the galactic system. However, its classification as a globular cluster has been challenged making it a candidate for being the stripped core of an accreted dwarf galaxy; this together with the fact that it has one of the largest velocity dispersions for star clusters in our galaxy makes it an interesting candidate for harboring an intermediate mass black hole. We measure the surface brightness profile from integrated light on an *HST*/ACS image of the center, and find a central power-law cusp of logarithmic slope -0.08. We also analyze Gemini GMOS-IFU kinematic data for a 5x5″ field centered on the nucleus of the cluster, as well as for a field 14″ away. We detect a clear rise in the velocity dispersion from 18.6 km s^{-1} at 14″ to 23 km s^{-1} in the center. A rise in the velocity dispersion could be due to a central black hole, a central concentration of stellar remnants, or a central orbital structure that is radially biased. We discuss each of these possibilities. An isotropic, spherical dynamical model implies a black hole mass of $4.0^{+0.75}_{-1.0} \times 10^4 M_\odot$, and excludes the no black hole case at greater than 99% significance. We have also run flattened, orbit-based models and find similar results. While our preferred model is the existence of a central black hole, detailed numerical simulations are required to confidently rule out the other possibilities.

Subject headings: globular clusters:individual(ω Centauri), stellar dynamics, black hole physics

1. Introduction

The globular cluster ω Centauri (NGC 5139) is regarded to be the largest and most massive member of the Galactic cluster system with a tidal radius of 69 parsecs (Harris 1996), an estimated mass of $5.1 \times 10^6 M_\odot$, and a measured central velocity dispersion of 22 ± 4 km s^{-1} (Meylan et al. 1995). The cluster presents a large scale global rotation, measured with radial velocities, of 8 km s^{-1} at a radius of 11pc from the center (Merritt et al. 1997) and confirmed with proper motions (van Leeuwen et al. 2000), which makes it one of the most flattened galactic globular clusters (White & Shawl 1987). A rotating flattened model including proper motion and radial velocity datasets by van de Ven et al. (2006) calculate a lower total mass of $2.5 \times 10^6 M_\odot$ and confirm the central line of sight velocity dispersion value of 20 km s^{-1}. They measure a dynamical distance of 4.8 ± 0.3 kpc (which we adopt for this paper). ω Cen has a peculiar highly bound retrograde orbit (Dinescu et al. 2001). It also has a stellar population that makes it stand out from the rest of the Galactic globular clusters due to its complexity. It shows a broad metallicity distribution (Bedin et al. 2004; Norris et al. 1996), as well as a kinematical and spatial separation between the different subpopulations (Pancino et al. 2003; Norris et al. 1997).

All the above results have led to the hypothesis that ω Cen is not a classical globular cluster, but instead is the nucleus of an accreted galaxy (Freeman 1993; Bekki & Freeman 2003; Meza et al. 2005). The scenarios of it being the product a merger of two globular clusters (Icke & Alcaino 1988) and of self-enrichment (Ikuta & Arimoto 2000) have also been proposed to explain the stellar populations.

The high measured velocity dispersion together with the possibility of being a stripped galaxy make ω Cen an interesting candidate for harboring a black hole in its center. The extrapolation of $M_\bullet - \sigma$ relation for galaxies (Gebhardt et al. 2000a; Ferrarese & Merritt 2000; Tremaine et al. 2002) predicts a $1.3 \times 10^4 M_\odot$ black hole for this cluster. The sphere of influence of such black hole for a star cluster at the distance of ω Cen with a velocity dispersion of 20 km s^{-1} is $\sim 5''$, making it an excellent target for ground-based observations.

Two globular clusters have been suggested for harboring an intermediate mass black hole in their nucleus. One is the galactic cluster M15 (Gebhardt et al. 2000b; Gerssen et al. 2002, 2003) and the other is G1, a giant globular cluster around M31 (Gebhardt et al. 2002, 2005). M15 is assumed to be in a post-core collapse state, therefore its dynamical state has been debated between harboring a black hole or containing a large number of compact remnants in its center (Baumgardt et al. 2003b,a). Unfortunately, observational constraints between these two hypothesis remain inconclusive (van den Bosch et al. 2006). G1 on the other hand, has a core with characteristics closer to those of ω Cen, and observations support the black hole interpretation for G1. Baumgardt et al. (2003c) propose an alternative interpretation

for G1 in which they match the observations with a model of two colliding globular clusters. The G1 black hole models are preferred since the M/L profile is expected to be flat in its core, so any rise in the velocity dispersion is unlikely to be due to remnants that concentrated there from mass segregation. The black hole interpretation for G1 is strongly supported by radio (Ulvestad et al. 2007) and x-ray (Pooley & Rappaport 2006) detections centered on the nucleus. ω Cen and G1 have similar properties in both their photometric and kinematic profiles. In this paper we report photometric and kinematical measurements that suggest the presence of a central black hole in ω Cen.

2. Surface Brightness Profile

The surface density profile at large radii for ω Cen has been measured from a combination of star counts and aperture photometry from ground based images (Meylan 1987; Trager et al. 1995; van Leeuwen et al. 2000). We measure the central part of the profile taking advantage of *Hubble Space Telescope* (*HST*) spatial resolution. We measure integrated light from an ACS F435W image (340 sec) applying the technique described in detail in Noyola & Gebhardt (2006), which uses a robust statistical estimator, the bi-weight, to calculate number of counts per pixel on a given annulus around the center of the cluster. As a test, we also measure the profile from a narrow band H-alpha image from the Rutgers Fabry-Perot (Xie et al. 2006) with lower spatial resolution. Since both images have a limited radial coverage, we use the Chebychev fit of Trager et al. (1995) for the surface brightness profile to cover the full, radial extent of the cluster. All profiles are normalized to the Trager profile.

Having accurate coordinates for the center of the cluster is crucial when measuring density profiles. Using the wrong center typically produces a shallower inner profile. We use a technique where we take an initial guess center, divide the cluster in eight concentric sectors around this center, and calculate the standard deviation of the sum of stars for the eight sectors. The radius of the sectors is chosen to be as large as the image will allow, in this case it is $\sim 2'$. We repeat the procedure for a grid of center coordinates and use the one that has the minimum standard deviation. Details about the technique can be found in Noyola & Gebhardt (2006). The coordinates for our center are RA $13 : 26 : 46.043$ and DEC $-47 : 28 : 44.8$ on the ACS dataset J6LP05WEQ using its WCS zeropoint.

The measured profiles from the B-band and H-alpha images are consistent as can be seen on Figure 1. The H-alpha profile follows the turnover around the core radius very well up to $100''$ and it also shows the rise toward the center, but it is noisier than the ACS profile. The solid line is a smooth fit made to the combination of the photometric points from ACS inside

$40''$ and Trager et al. Chebychev fit outside $40''$. For comparison, we include the Trager et al. (1995) photometric points in the plot. The surface brightness profile shows a continuous rise toward the center with a logarithmic slope of -0.08 ± 0.03, which is in contrast to the common notion that ω Cen has a flat core. Van Leeuwen et al (2000) perform star counts for giant stars and notice that they are more concentrated than previously thought. Our result is consistent with their finding. Baumgardt et al. (2005) perform N-body models of star clusters with initial King profiles and containing a central black hole. They predict the formation of a shallow cusp of -0.1 to -0.3 logarithmic slope after $1.5 - 4$ relaxation times. Trenti et al. (2007) perform similar N-body models and conclude that clusters containing central IMBHs evolve to configurations that have extended cores, with $r_c/r_h \sim 0.3$. The r_c/r_h ratio for ω Centauri is 0.33, which is in very good agreement with the predictions from this models. Our observed surface brightness profile is intriguing considering that it follows the two specific predictions from these N-body models, but of course, only kinematical measurements can determine the mass profile, and test the existence of a central black hole.

3. Kinematic Measurements

Obtaining kinematic information of the central regions of Galactic globular clusters is a challenging task since the brightest stars dominate with typical ground-based conditions and the extreme crowding produces confusion. Measuring individual radial velocities requires a spatial resolution that can only be achieved with adaptive optics or from space. On the other hand, measuring velocity dispersion from an integrated spectrum is subject to shot noise due to giant stars whose contribution dominates the light. Dubath et al. (1997) calculate the relative contribution to integrated light by different stellar groups. They find that the contribution from the few brightest stars is equal in weight to that of the much larger numbers of fainter stars. Therefore, the only way to obtain accurate radial velocity dispersion measurements from an integrated spectrum is if the participation of the brightest stars can somehow be avoided or at least minimized. One way to do this is by observing crowded regions with an integral field unit (IFU) which produces individual spectra of subsections in the region (typically $\sim 0.2''$ in size). One can exclude the spectra affected by the brightest stars when measuring the integrated background light and thus decrease the shot-noise contribution to the uncertainty. The Gemini telescopes operate primarily using a queue scheduling, which makes them an excellent tool to measure integral field spectra of globular clusters since observing constraints (such as excellent seeing) can be specified in advance, and data is only taken when the required observing constraints are met.

As part of the Science Verification program for the Gemini GMOS-South IFU, we ob-

tained nod-and-shuffle observations on February 29 2004 (program ID: GS-2003B-SV-208). We use the IFU in 2-slit nod-and-shuffle mode, which gives a field of view of $5'' \times 5''$, comprised of 700 individual lenslets plus fiber elements, each of which covers approximately $0''.2$ on the sky. We use the R600 grating, yielding a resolving power R=5560, which we measure from the lamp spectral lines, along with the Calcium Triplet filter to give a wavelength coverage of 7900-9300Å. Three fields are observed, each for a total integration time of 900 sec on source and 900 sec on sky. The observations are made using the nod-and-shuffle technique with 30 sec sub-integrations observed in a B-A-A-B pattern, where A is the on-source position and B is the sky position, located $498''$ away. The nod-and-shuffle technique improves the sky subtraction, especially in the presence of CCD fringing, by sampling the object and sky on exactly the same CCD pixels, with exactly the same light path, on timescales comparable to those of the sky emission line variability. The first of the three fields is located at the cluster center, and the second field is centered $14''$ away. The third field appears to have been pointing somewhere else but, despite much efforts, we cannot determine exactly where the IFU observations are pointed (they do not match anything in the acquisition image for this field). The reconstructed IFU image for this third field contains fewer stars and the PSF is obviously broader than for the other two. It is clear that the exposure was taken during much worse seeing conditions than the other two fields, so shot-noise effects are likely to be important; for this reasons we exclude the third field from further analysis. Using the standard tasks from the IRAF-GEMINI package we sky subtract, flat-field, and extract the spectra for each fiber and apply a wavelength calibration.

The standard flat subtraction does not remove all of the fringing pattern in the image. As a result, a constant number of counts have to be subtracted from the data frames before flattening in order to reduce fringing problems. Relative to the bias frame, the amount of additional counts from scattered light is about 8%. Even after this procedure, there is some residual fringing that can only be alleviated by combining individual fibers over the full field into one spectrum. To combine individual fibers we first divide by the continuum. The intention is to de-weight the bright stars with respect to the fainter ones, which helps to lessen the problems due to shot noise. For the continuum fit, we run a boxcar of dimension 111×1 over the reduced image, and then divide the central pixel by the median of the pixels in the box. This procedure brings all spectra to the same continuum level. We then combine every individual fiber with the six adjacent ones, since this represents one seeing disk for the observations

Figure 2 shows the reconstructed image from the IFU fibers for the central frame and the acquisition image as well as the same region on the ACS image. We also show a convolved image (with the reported seeing for the observations) of the ACS frame. The same match is performed for the field $14''$ away (Fig 3). Both ACS fields contain ~ 100 resolved stars. We

construct a luminosity function for the detected stars for each field and compare it to the luminosity function of the entire cluster core. The luminosity function is consistent between the two fields. The brightest stars detected in both fields are two magnitudes fainter than the brightest stars detected in the core of the cluster. This excludes the possibility of the integrated spectra being artificially broadened by the presence of more blue straggler stars in the central field compared to the field $14''$ away. Using the photometric measurements of individual stars together with the reported seeing, we calculate how many stars contribute to each fiber. Excluding the fibers which are dominated by a single star we estimate that the integrated spectrum of the background unresolved light represent about 60 stars in both fields.

We focus on the Ca triplet region (8450Å-8700Å) for our analysis. We measure the relative velocities between each fiber for the two fields and obtain velocity distributions from the individual fiber velocities. We fit a Gaussian to the velocity distributions and observe that the one for the central field is clearly broader than for the one $14''$ away. The largest relative velocity between two fibers is 80 km s^{-1} for the central frame, and 60 km s^{-1} for the other one. Using the dispersion of the individual fiber velocities as a measure of the cluster velocity dispersion will be biased. Since multiple stars, in general, provide light to an single fiber, the measured velocity in that fiber will be pulled toward the cluster mean as opposed to representing one star. Thus, the dispersions of the fiber velocities will be biased significantly low. This is what we find although the central frame does have a obviously larger spread in fiber velocities.

To properly estimate the velocity dispersion we have to rely on the integrated light, and require template stars in this case. Unfortunately, we do not have isolated stars that are free from the fringe problems mentioned earlier, so we cannot accurately use template stars observed with the same instrument. We rely on the template stars observed by Walcher et al. (2005), from VLT-UVES observations at around R=35000. We convolve the spectra to our measured resolving power. To extract the velocity dispersion from the integrated light we utilize the non-parametric, pixel-based technique as described in (Gebhardt et al. 2000c; Pinkney et al. 2003). We choose an initial velocity profile in bins, convolve it with the template (or set of templates), and calculate residuals to the integrated spectrum. The parameters for the line of sight velocity distribution (either velocity bin values or, if desired, a parametric Gauss-Hermite expansion) are varied to provide the best match. Monte Carlo simulations determine the uncertainties, and use the measured noise in the spectrum.

The dispersion fitting routine allows for a mismatch in the equivalent width between the object and template. In this case, there is a 30% difference in the equivalent width of the calcium triplet lines. We do not know whether this is caused by the scattered light (unlikely

given the amplitude), the specific templates we used, omega Cen's particular composition, or a combination of all three. We have run a variety of tests to determine whether stars of difference equivalent widths would cause a bias in dispersions, and find no such bias. We have also measured the dispersions using template stars from the same IFU data, since there is at least one star that is fairly isolated. The uncertainties are larger due to the scattered light problems, but the value of the dispersion remains the same. Thus, we conclude that template issues are not a significant source of bias in the dispersion estimate.

We combine the spectra from individual fibers using a biweight estimator. Different sets of fibers for each frame are combined in order to test for consistency in our results. First, we combine every fiber on the frame, then we exclude the 25%, 50% and 75% brightest fibers. We measure the velocity dispersion for these four spectra for each frame. The measured velocity for the central frame is always higher than the one for the frame $14''$ away for every equivalent pair of combined spectra. We measure velocity dispersions from 21.8 to 25.2 km s^{-1} for the central field, and 18.2 to 19.1 km s^{-1} for the field $14''$ away. We adopt 23.0 ± 2.0km s^{-1} for the central field and 18.6 ± 1.6km s^{-1} for the other. The latter measurement coincides with the central velocity dispersion value measured for ω Cen by various authors. Van den Ven et al. (2006) measure a line of sight velocity dispersion profile by combining various datasets (Suntzeff & Kraft 1996; Mayor et al. 1997; Reijns et al. 2006; Xie et al. 2006). They use 2163 individual radial velocity measurements divided into polar apertures to obtain the final velocity dispersion profile. We use dispersion estimates as presented in their table 4. The average radius for the spectra that contribute to the central values is $2.5''$ and $14''$ for the second. Figure 4 presents the velocity dispersion data.

4. Models

As discussed in Section 2, the central shape of the surface brightness profile of ω Cen resembles that found by Baumgardt et al. (2005) in star clusters harboring black holes. The presence of an intermediate black hole at the center of this cluster is one of the possibilities for explaining the observed rise in velocity dispersion. We have run two types of modeling: 1) spherical and isotropic, and 2) flattened, orbit-based models that allow for general anisotropy. Although the orbit-based models are more general, they do not consider dynamical stability. For a system with a half light relaxation time shorter than its age, like ω Cen, the dynamical evolution cannot be ignored. Therefore, while the two models give similar results we quote results from the isotropic analysis and use the orbit-based models to explore possible velocity anisotropies.

For the isotropic analysis, we create a series of models using the non-parametric method

described in Gebhardt & Fischer (1995). As a first step we apply a reddening correction to the observed surface brightness profile. Harris (1996) reports a 0.1 reddening for this cluster, which, although being relatively low, it is important for the proper M/L determination of the models. The reddening correction will only affect the M/L value of the models, but not the shape of the profiles. We deproject the surface brightness profile using Abel integrals assuming spheroidal symmetry. The integral involves a derivative of the profile, therefore, any amount of noise present is amplified. We apply a spline smoother to the surface brightness profile before deprojecting and thus obtain a luminosity density profile as discussed in Gebhardt et al. (1996). By assuming an M/L ratio, we calculate a mass density profile, from which the potential and the velocity dispersion can be derived. We repeat the calculation adding a variety of central point masses ranging from 0 to $7.5 \times 10^4 M_\odot$ while keeping the global M/L value fixed. Van de Ven et al (2006) measure a fairly constant stellar M/L profile for ω Cen of 2.5 ± 0.1. We find a constant mass luminosity ratio of 2.7, since this provides the best match to the observed velocity dispersion profile outside the core.

Figure 4 shows the comparison between the different models and the measured dispersion profile. The most relevant part of the comparison is the rise inside the core radius, in particular the rise between the two innermost measurements. As it can be seen, an isotropic model with no black hole present predicts a slight decline in velocity dispersion toward the center, instead we observe a clear rise. The predicted central velocity for the no black hole model is 14.6 km s^{-1} which is well below any line of sight velocity dispersion measured inside $1'$. The calculated χ^2 values for each model are plotted in Figure 5, as well as a line showing a $\Delta\chi^2 = 1$. The χ^2 curve implies a best-fitted black hole mass of $4^{+0.75}_{-1} \times 10^4 M_\odot$. Even the original velocity dispersion profile without our two innermost measurement already points to an intriguing discrepancy, but the central measurements confirm an important rise in M/L from the core radius to the center of this cluster. The central M/L value is 6.7, which is a considerable rise from the value of 2.7 just inside the core radius. Our best fit model implies a central density of $5.6 \times 10^7 M_\odot/pc^3$ the largest measured in a globular cluster.

We also construct axisymmetric orbit-based dynamical models. The models are based on the formulation by Schwarzschild (1979) and are constructed as in Gebhardt et al. (2000c, 2003). These models provide the most freedom possible of the distribution function for an axisymmetric system. We use the same deprojection as describe above, except we also include the observed flattening. Assuming an M/L ratio and a BH mass, the mass distribution of the cluster is obtained and from it, the potential can be computed. Using this potential, we generate about 10^4 representative orbits. The best match to the observed photometric and kinematical data provide the orbital weights for a given potential. The process is repeated for various M/L values and BH masses until the minimum χ^2 model is found. The kinematical observations matched here are the individual radial velocities from van den Ven et al. (2006),

and the two integrated measurements described above. We plan to perform more detailed orbit-based models including proper motion measurements in the future.

Figure 7 plots χ^2 as a function of black hole mass and stellar M/L. The best fit model requires a black hole mass of $3 \pm 1 \times 10^4 \ M_\odot$, with 1-sigma of the isotropic result. As expected, since orbit-based models are more general, the difference in χ^2 compared to the no black hole case is smaller than in the isotropic case. The $\Delta\chi^2$ between the best-fitted black hole model and no black hole model is 4 (marginalized over M/L), implying a 95% significance. In comparison, the χ^2 difference for the isotropic models is 25. As discussed below, the reason for the difference is that the orbit-based models allow for significant radial anisotropy in the core for the no black hole model, while the best-fitted mass produces a nearly isotropic distribution consistent with previous measurements (van de Ven et al. 2006).

We also plot the velocity dispersion profile as measured in the best-fit orbit based model in Figure 4, given as the dashed (red) line. The dispersion profile for the orbit-based model with no black hole is very similar, with no obvious correlated differences. The reason there are no obvious differences is because the overall change in χ^2 is small and the orbit-based models tend to redistribute orbital weights to spread χ^2 over the full radial range. As discussed in Gebhardt et al. (2003), it is difficult to see differences in radial profiles of projected kinematics between models with black holes and without, even for galaxies where the overall χ^2 difference is large. This is understood since the orbit models have the freedom to change the orbital properties in such a way to even out the χ^2 differences over the full spatial extent of the observations. For omega Cen, the black hole model only provides an increase in χ^2 of 4; thus with 23 data points, the average difference in terms of the meaurement uncertainty is 0.42. For these reasons, the orbit-based models provide a modest significance for a black hole, and the argument is significantly strengthened when considering the need for the strong amount of radial anisotropy when a black hole is not included.

The observations we use in the dynamical modeling rely on only the first and second moments of the velocity distribution. Since we have individual velocities (except for the central two radial points), we can utilize the full velocity profile. Furthermore, proper motion data exists for data at larger radii (van den Ven et al. 2006). Including both effects, full velocity profiles and proper motions, will be the subject of a more detailed paper on omega Cen.

4.1.   Alternative to a Black Hole: Dark Remnants

A possible alternative to explain the observed rise in M/L toward the center is a concentration of dark stellar remnants, e.g. neutron stars, stellar mass black holes, or massive white dwarfs. Using the observed velocity dispersion profile, we calculate the total enclosed mass and from this, the mass density profile. We then compare this with the enclosed mass implied by the luminosity density profile, assuming the same M/L as for the models in the previous section. From these two profiles, we can estimate the density profile of the implied extended dark component, if we assume this was the cause of the velocity dispersion rise towards the center. Figure 6 shows the estimated density profile for the dark and luminous components. It is clear that, if the velocity rise is due to an extended distribution of dark stellar remnants, the density profile of this dark component needs to be very concentrated and steep, with a logarithmic slope of ~ -2.0 (the slope of the dashed line in the figure), resembling a cluster undergoing core collapse. The relaxation time for ω Cen implies a much slower dynamical evolution than the one necessary to reach such a configuration. Core-collapse models have shown that when a cluster has reached such a high degree of mass segregation, the observable core to half light radius gets very small, with values below 0.05 (Breeden et al. 1994; Makino 1996), while this ratio is 0.3 for ω Cen. Also, the concentration value for ω Cen is $c = 1.6$ (Harris 1996), which is too low a value for the cluster to have undergone core-collapse. No evolutionary model predicts such a concentrated distribution of dark remnants inside a cluster with a shallow extended core for the visible stars. Furthermore, the required number of dark remnants is around 1% of the cluster mass. While this number is expected from stellar evolution, it is not expected to have all of the remnants to be concentrated inside of the core.

4.2.   Alternative to a Black Hole: Orbital Anisotropy

Another possibility is that the observed rise in velocity dispersion is due to velocity anisotropy in the cluster. The orbit-based models explore this possibility. The two main results from the orbit analysis are that 1) the lowest χ^2 model is the one with a central black hole and 2) the model with no black hole requires a substantial amount of radial anisotropy. Figure 8 shows that without the presence of a central black hole, a large degree of radial anisotropy – σ_r/σ_t=1.5 – is required inside 0.3 r_c. At $r > 28''$, the models with and without a black hole are close to isotropic, in agreement with the results of van den Ven et al. (2006). For a system as dense as ω Cen, such a degree of anisotropy as measured in the no black hole case is expected to be quickly erased through relaxation processes. However, even with such a strong amount of radial anisotropy, the no black hole case is a poorer fit than the best-fitted

black hole. One of the disadvantages of the orbit-based models is that we cannot include the dynamical stability arguments in the χ^2 analysis, and for a system with a short relaxation time such as a globular cluster, this may be important. We, therefore, adopt results from the isotropic models, in particular since the analysis of van den Ven et al. (2006) find an isotropic distribution.

5. Discussion

We measure the surface brightness profile for the globular cluster ω Centauri (NGC 5139) from an ACS image in the central $40''$. The profile shows a continuous rise toward the center with a logarithmic slope of -0.08 ± 0.03, in contrast with previous measurements which found a flat core. The shape of the profile is similar to that obtained from numerical models of star clusters containing black holes in their centers. We measure a line of sight velocity dispersion for two $5'' \times 5''$ regions, one at the center of the cluster and the other $14''$ away. We detect a rise in velocity dispersion from 18.6 km s^{-1} for the outer field to 23 km s^{-1} for the central one. We combine these two measurements with previously measured velocity dispersion at larger radii.

When we compare the observed velocity dispersion profile with a series of isotropic models containing black holes of various masses, we find that a black hole of $4.0^{+0.75}_{-1.0} \times 10^4 M_\odot$ is necessary to match the observations. We explore alternative explanations for the observed rise in our central velocity dispersion measurements. First we consider the possibility that the observed M/L rise is due to the presence of an extended component composed of dark remnants such as neutron stars or faint white dwarfs. The density profile of the dark component is required to be extremely concentrated toward the center, with a configuration practically decoupled from the luminous component. ω Cen has a weak cusp in the central luminosity density profile, implying that the gravitational potential is very shallow inside the core and therefore mass segregation is only a weak effect. Ferraro et al. (2006) confirm the lack of segregation by measuring the radial distribution of blue straggler stars, which are heavy stars and should sink to the center of the cluster if there is mass segregation. They find a flat radial distribution of blue stragglers with respect to lighter stellar populations. Also, the formation channel of the blue stragglers is not collisional, as it would be expected if there was a considerable amount of mass segregation. With this evidence in hand, there is no reason to expect a large variation of M/L inside the core due to stellar content, so a detected rise in M/L is likely to come from the presence of a concentrated massive object.

There is also a stability argument against a dense compact cluster of dark remnants. The central density as measured from the 23 km s^{-1} dispersion estimate at $1.8''$ is $5.6 \times 10^7 M_\odot/pc^3$.

This is the largest measured for a globular cluster and it would be difficult to maintain using stellar remnants. Obviously, if the density is due to solar mass remnants, over 10^4 remnants would be required inside of 0.05 parsecs. Using the arguments of Maoz (1998) and Miller (2006), this mass and density makes ω Cen one of the better examples where stellar remnants can be ruled out due to evaporation. Maoz estimates that for these numbers, any cluster of remnants will have evaporated within the age of the cluster.

An observed velocity dispersion rise toward the center of a cluster can also occur if a degree of anisotropy is present. If more radial orbits are present, those stars pass near the center at higher velocities than they would in an isotropic case. This possibility is evaluated with our orbit-based models. Our results agree with the model by van den Ven et al. (2006) in showing no anisotropy in the central 10 arcmin. Their models show a degree of tangential anisotropy at large radius, but no radial anisotropy. Models without a central black hole but having a large degree of anisotropy inside 28″ are not as as good as models including a black hole. Furthermore, the high degree of radial anisotropy is highly unstable in dense systems like ω Cen and therefore it is an unlikely explanation for the observed kinematics.

Figure 9 shows the known $M_\bullet - \sigma_v$ relation for black holes in elliptical galaxies and bulges (Gebhardt et al. 2000a; Ferrarese & Merritt 2000). The galaxies used to determine the relation (Tremaine et al. 2002) are plotted along with objects containing smaller black holes in low luminosity quasars (Barth et al. 2005), two nearby low luminosity AGN (NGC 4595 and Pox 52), and three globular clusters (G1, M15 and ω Cen). We also plot the upper limit for the black hole mass in the nucleus of M33 (Gebhardt et al. 2001), which does not lie on the correlation. The black hole in ω Cen lies above the relation, but it is consistent with the scatter observed a larger masses. The measured black hole mass is 1.6% of the total mass of the cluster, which is much larger than the canonical value of $\sim 0.3\%$ for larger spheroids (Magorrian et al. 1998). If ω Cen is indeed the nucleus of an accreted galaxy it is expected that it's original mass was considerably larger than what we measure now. Bekki & Freeman (2003) reproduce the current mass and orbital characteristics of ω Cen with a model of an accreted $10^7 M_\odot$ dwarf galaxy. A mass of $4 \times 10^7 M_\odot$ for the original spheroid would put the black hole near the 0.3% value.

The two pieces of observational evidence that ω Cen could harbor a central black hole come from the photometry and the kinematics. From the HST image of ω Cen, we measure a central logarithmic surface brightness slope of -0.08 ± 0.03. This value is very similar to that claimed by the N-body simulations of Baumgardt et al. (2005) that are most likely explained by a central black hole. Standard core-collapse does not lead to such a large core with a shallow central slope. The black hole tends to prevent core collapse while leaving an imprint of a shallow cusp. It will be important to run models tailored to ω Cen to see if

– 13 –

one can cause and maintain a shallow cusp without invoking a central black hole. However, the main observational evidence for the central mass comes from the increase in the central velocity dispersion, where we detect a rise from 18.6 to 23 km s^{-1} from radii of 14 to 2.5″. In fact, even excluding the Gemini data presented here, the previous ground-based data suggest a central mass concentration as well. The core of ω Cen is around 155 ″ (about 2.5 ′), so the dispersion rise is seen well within the core.

REFERENCES

Barth, A. J., Greene, J. E., & Ho, L. C. 2005, ApJL, 619, L151

Baumgardt, H., Heggie, D. C., Hut, P., & Makino, J. 2003a, MNRAS, 341, 247

Baumgardt, H., Hut, P., Makino, J., McMillan, S., & Portegies Zwart, S. 2003b, ApJL, 582, L21

Baumgardt, H., Makino, J., & Hut, P. 2005, ApJ, 620, 238

Baumgardt, H., Makino, J., Hut, P., McMillan, S., & Portegies Zwart, S. 2003c, ApJL, 589, L25

Bedin, L. R., Piotto, G., Anderson, J., Cassisi, S., King, I. R., Momany, Y., & Carraro, G. 2004, ApJL, 605, L125

Bekki, K., & Freeman, K. C. 2003, MNRAS, 346, L11

– 14 –

Breeden, J. L., Cohn, H. N., & Hut, P. 1994, ApJ, 421, 195

Dinescu, D. I., Majewski, S. R., & Girard, K. M., T. M. andCudworth. 2001, AJ, 122, 1916

Dubath, P., Meylan, G., & Mayor, M. 1997, AAP, 324, 505

Ferrarese, L., & Merritt, D. 2000, ApJL, 539, L9

Ferraro, F. R., Sollima, A., Rood, R. T., Origlia, L., Pancino, E., & Bellazzini, M. 2006, ApJ, 638, 433

Freeman, K. C. 1993, in ASP Conf. Ser. 48: The Globular Cluster-Galaxy Connection, 608

Gebhardt, K., et al. 2000a, ApJ, 539, L13

Gebhardt, K., & Fischer, P. 1995, AJ, 109, 209

Gebhardt, K., et al. 2001, AJ, 122, 2469

Gebhardt, K., Pryor, C., O'Connell, R. D., Williams, T. B., & Hesser, J. E. 2000b, AJ, 119, 1268

Gebhardt, K., Rich, R. M., & Ho, L. C. 2002, ApJ, 578, L41

Gebhardt, K., Rich, R. M., & Ho, L. C. 2005, ApJ, 634, 1093

Gebhardt, K., et al. 1996, AJ, 112, 105

Gebhardt, K., et al. 2000c, AJ, 119, 1157

Gebhardt, K., et al. 2003, ApJ, 583, 92

Gerssen, J., van der Marel, R. P., Gebhardt, K, Guhathakurta, P., Peterson, R. C., & Pryor, C. 2002, AJ, 124, 3270

Gerssen, J., van der Marel, R. P., Gebhardt, K., Guhathakurta, P., Peterson, R. C., & Pryor, C. 2003, AJ, 125, 376

Harris, W. E. 1996, AJ, 112, 1487

Icke, V., & Alcaino, G. 1988, AAP, 204, 115

Ikuta, C., & Arimoto, N. 2000, AAP, 358, 535

Magorrian, J., et al. 1998, AJ, 115, 2285

– 15 –

Makino, J. 1996, ApJ, 471, 796

Mayor, M., et al. 1997, AJ, 114, 1087

Merritt, D., Meylan, G., & Mayor, M. 1997, AJ, 114, 1074

Meylan, G. 1987, AAP, 184, 144

Meylan, G., Mayor, M., Duquennoy, A., & Dubath, P. 1995, AAP, 303, 761

Meza, A., Navarro, J. F., Abadi, M. G., & Steinmetz, M. 2005, MNRAS, 359, 93

Norris, J. E., Freeman, K. C., Mayor, M., & Seitzer, P. 1997, ApJL, 487, L187

Norris, J. E., Freeman, K. C., & Mighell, K. J. 1996, ApJ, 462, 241

Noyola, E., & Gebhardt, K. 2006, AJ, 132, 447

Pancino, E., Seleznev, A., Ferraro, F. R., Bellazzini, M., & Piotto, G. 2003, MNRAS, 345, 683

Pinkney, J., et al. 2003, ApJ, 596, 903

Pooley, D., & Rappaport, S. 2006, ApJ, 644, L45

Reijns, R. A., Seitzer, P., Arnold, R., Freeman, K. C., Ingerson, T., van den Bosch, R. C. E., van de Ven, G., & de Zeeuw, P. T. 2006, AAP, 445, 503

Schwarzschild, M. 1979, ApJ, 232, 236

Suntzeff, N. B., & Kraft, R. P. 1996, AJ, 111, 1913

Trager, S. C., King, I. R., & Djorgovski, S. 1995, AJ, 109, 218

Tremaine, S., et al. 2002, ApJ, 574, 740

Trenti, M., Ardi, E., Mineshige, S., & Hut, P. 2007, MNRAS, 374, 857

Ulvestad, J. S., Greene, J., & Ho, L. 2007, ApJL, accepted

van de Ven, G., van den Bosch, R. C. E., Verolme, E. K., & de Zeeuw, P. T. 2006, AAP, 445, 513

van den Bosch, R., de Zeeuw, T., Gebhardt, K., Noyola, E., & van de Ven, G. 2006, ApJ, 641, 852

van Leeuwen, F., Le Poole, R. S., Reijns, R. A., Freeman, K. C., & de Zeeuw, P. T. 2000, AAP, 360, 472

Walcher, C. J., et al. 2005, ApJ, 618, 237

White, R. E., & Shawl, S. J. 1987, ApJ, 317, 246

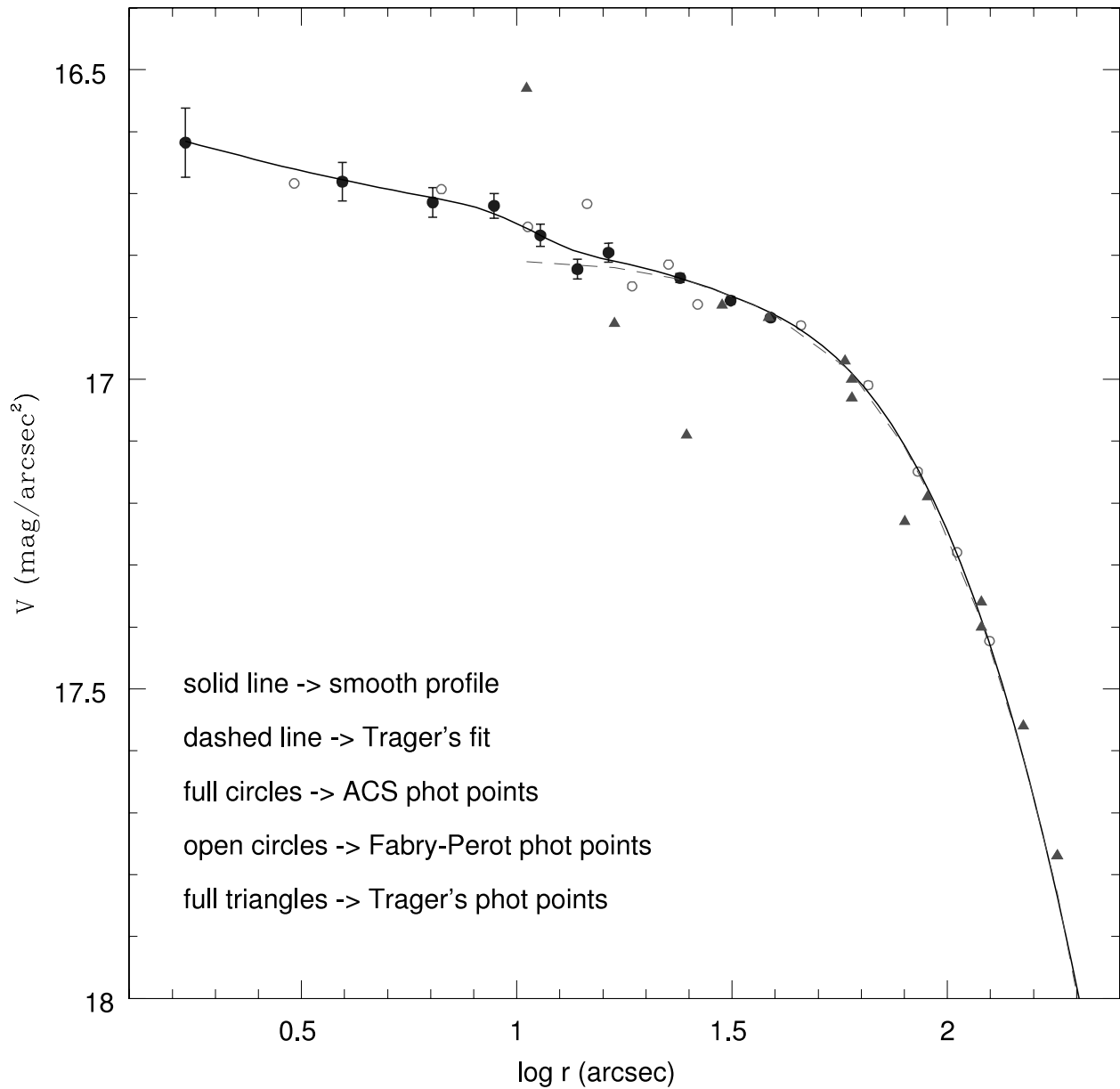Xie, B., Gebhardt, K., Pryor, C., & Williams, T. B. 2006, in prep

Fig. 1.— Surface brightness profiles for ω Cen. The circles show our measured photometric points from the ACS (filled) and H-alpha (open) images. The triangles show photometric points obtained from ground based images by Trager et al. The dashed line is Trager's Chebychev fit. The solid line is our smooth fit to the combination of the ACS points inside 40″ and Trager's Chebychev fit outside.
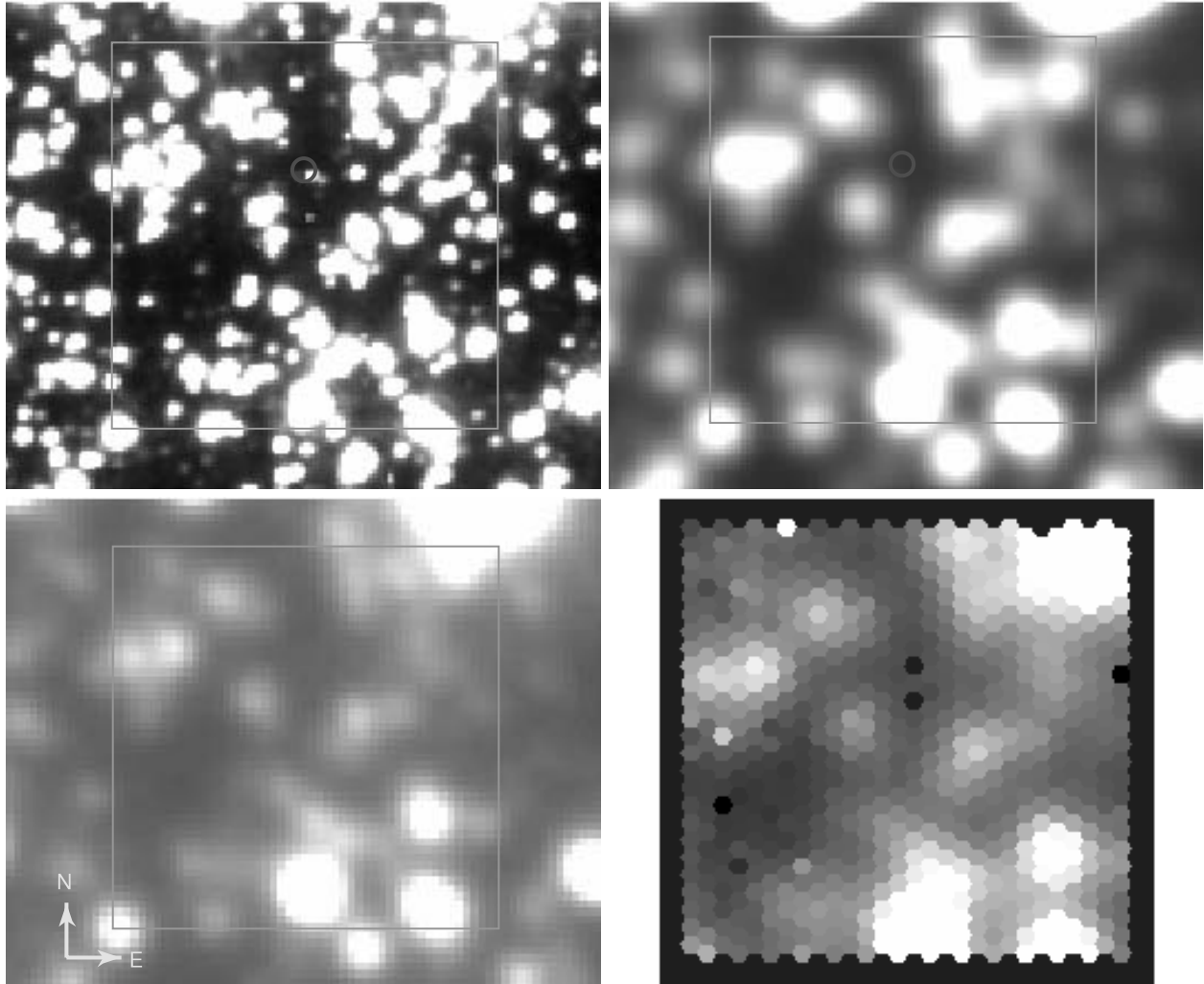
Fig. 2.— The central field observed with the GMOS-IFU. The green box represents the GMOS field of view. Top left: ACS image of the observed region. The red circle marks the center of the cluster. Top right: Convolved ACS image to reproduce the reported seeing during observations. Bottom left: GMOS acquisition image. Bottom right: Reconstructed GMOS-IFU image.
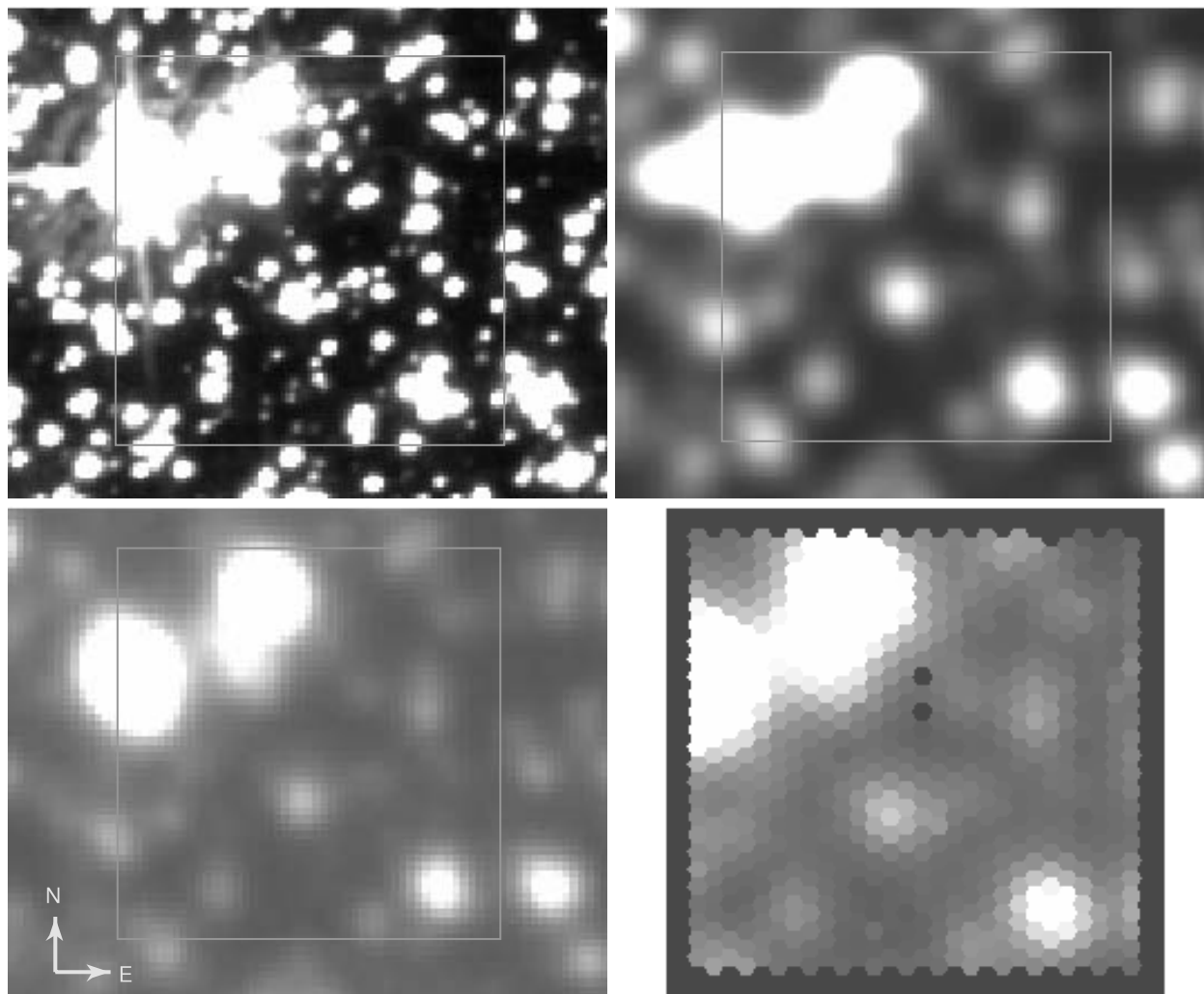
Fig. 3.— Same as fig 2 for the field 14″ away.
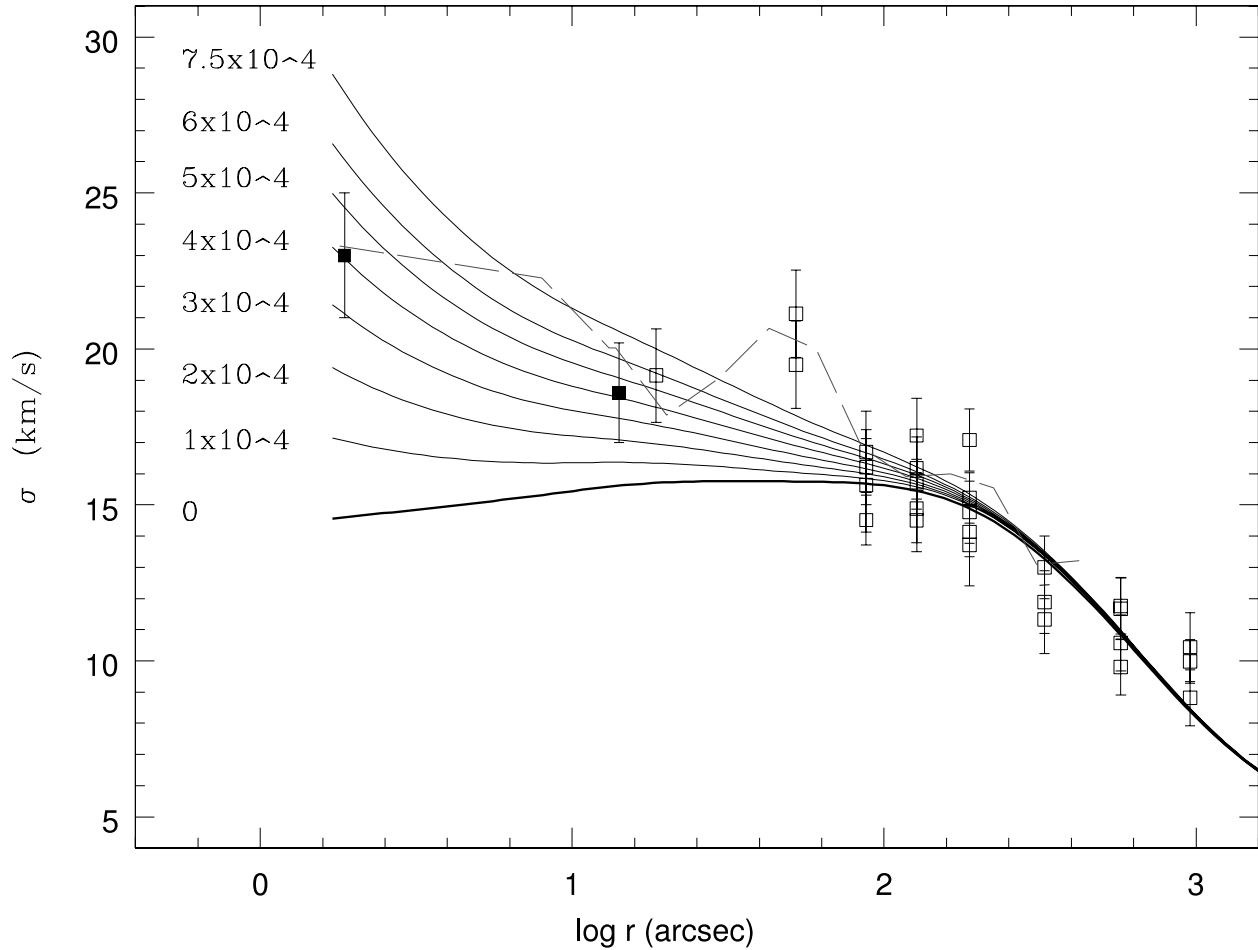
Fig. 4.— Velocity dispersion profile for ω Cen with various central black hole models. Filled squares are the dispersions and uncertainties from the GMOS-IFU and open circles are from individual radial velocity measurements. A set of isotropic spherical models of varying black hole masses is shown for comparison. The thick line is the no black hole model and the thin lines represent models with black holes as labeled. The dashed (red) line is the velocity dispersion profile for the best-fit orbit-based model (in Section 4).
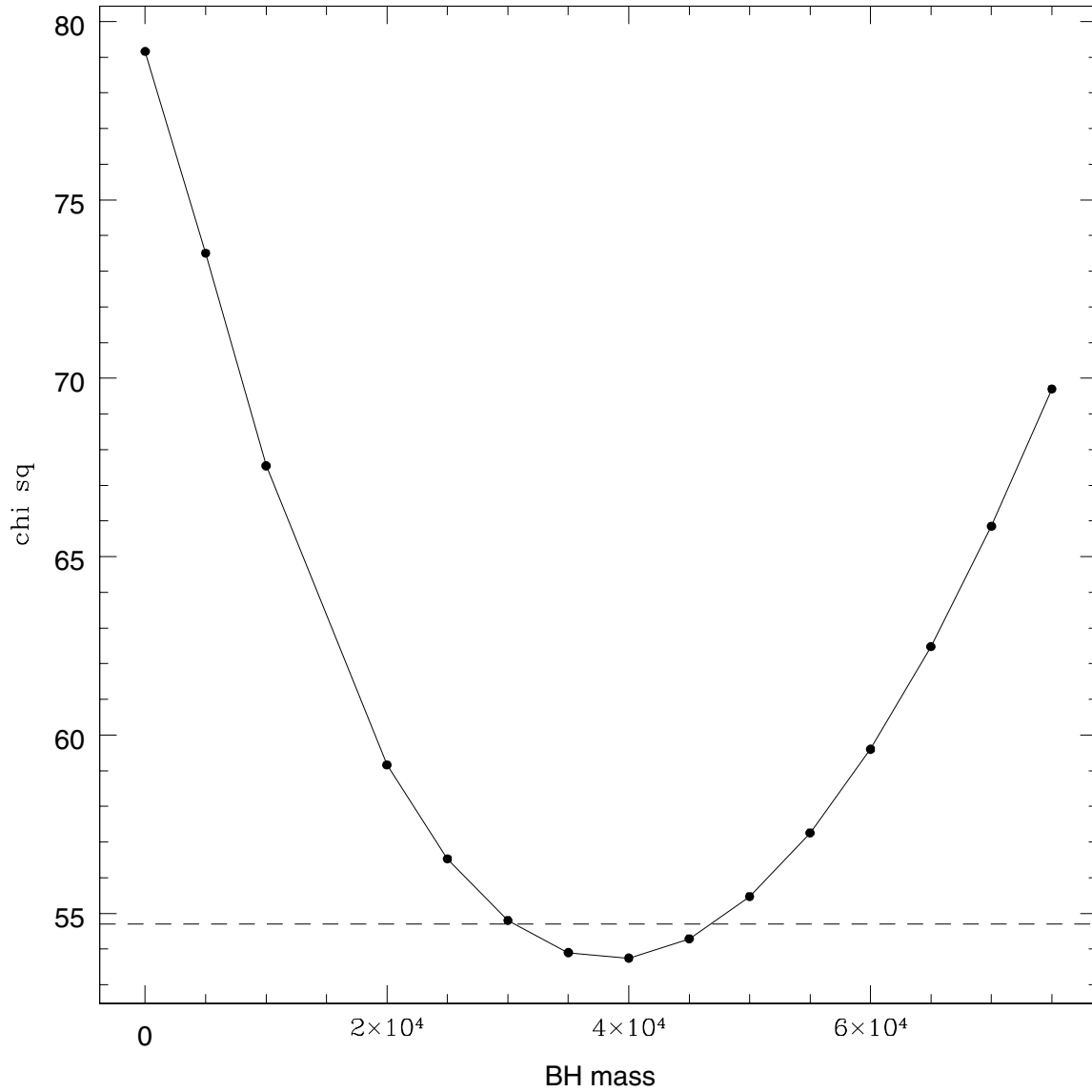
Fig. 5.— χ^2 vs. black hole mass. The minimum is found for a black hole mass of $4.0 \times 10^4 M_\odot$, with 68% confidence limit at 3 and $4.75 \times 10^4 M_\odot$ marked by the dashed line. For our model assumptions, the no black hole model is excluded at greater than the 99% confidence
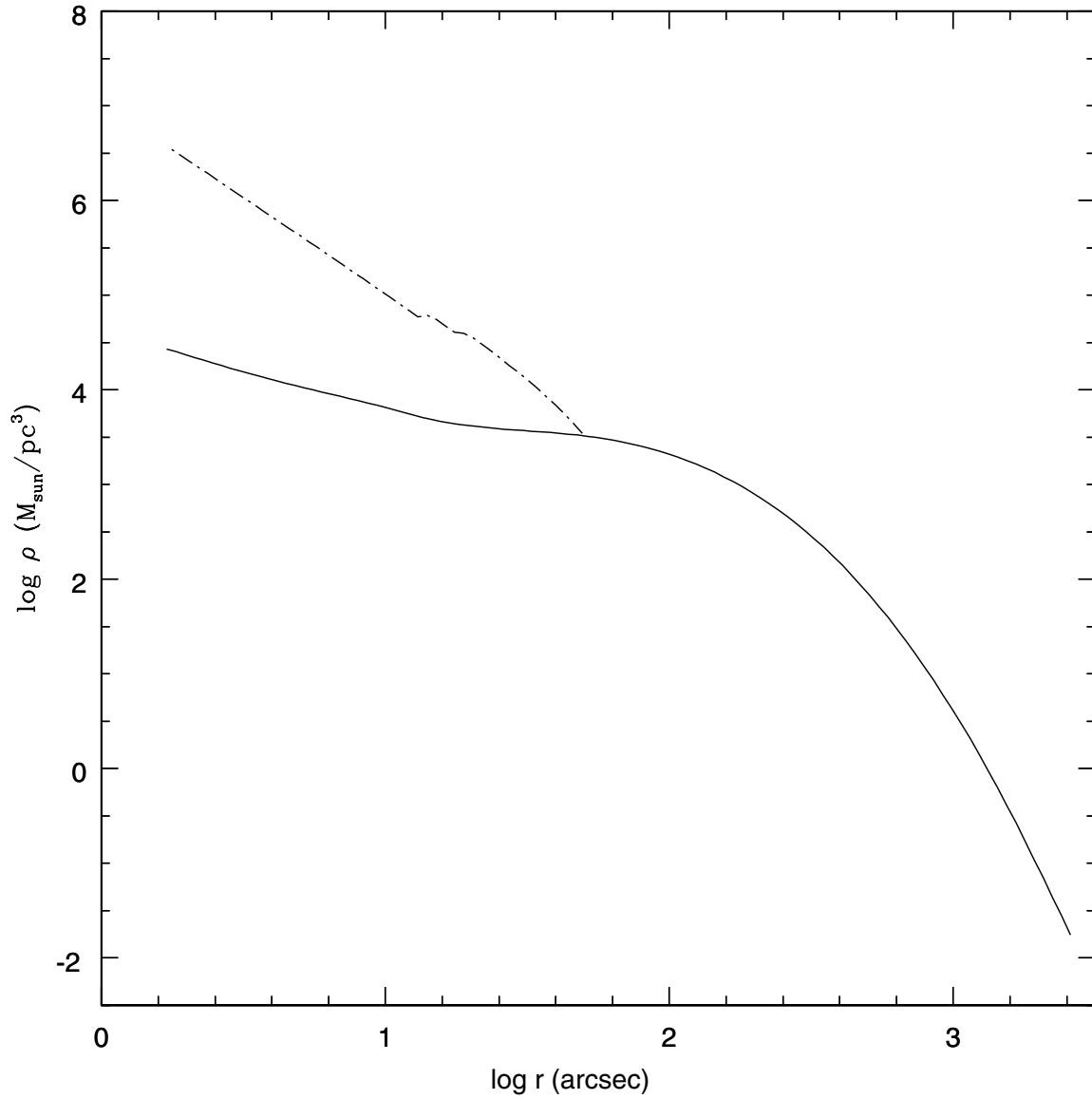
Fig. 6.— Inferred density profiles. The solid line is the deprojected density profile for the luminous component. The dashed line represents the required dark component to reproduce the observed kinematics.
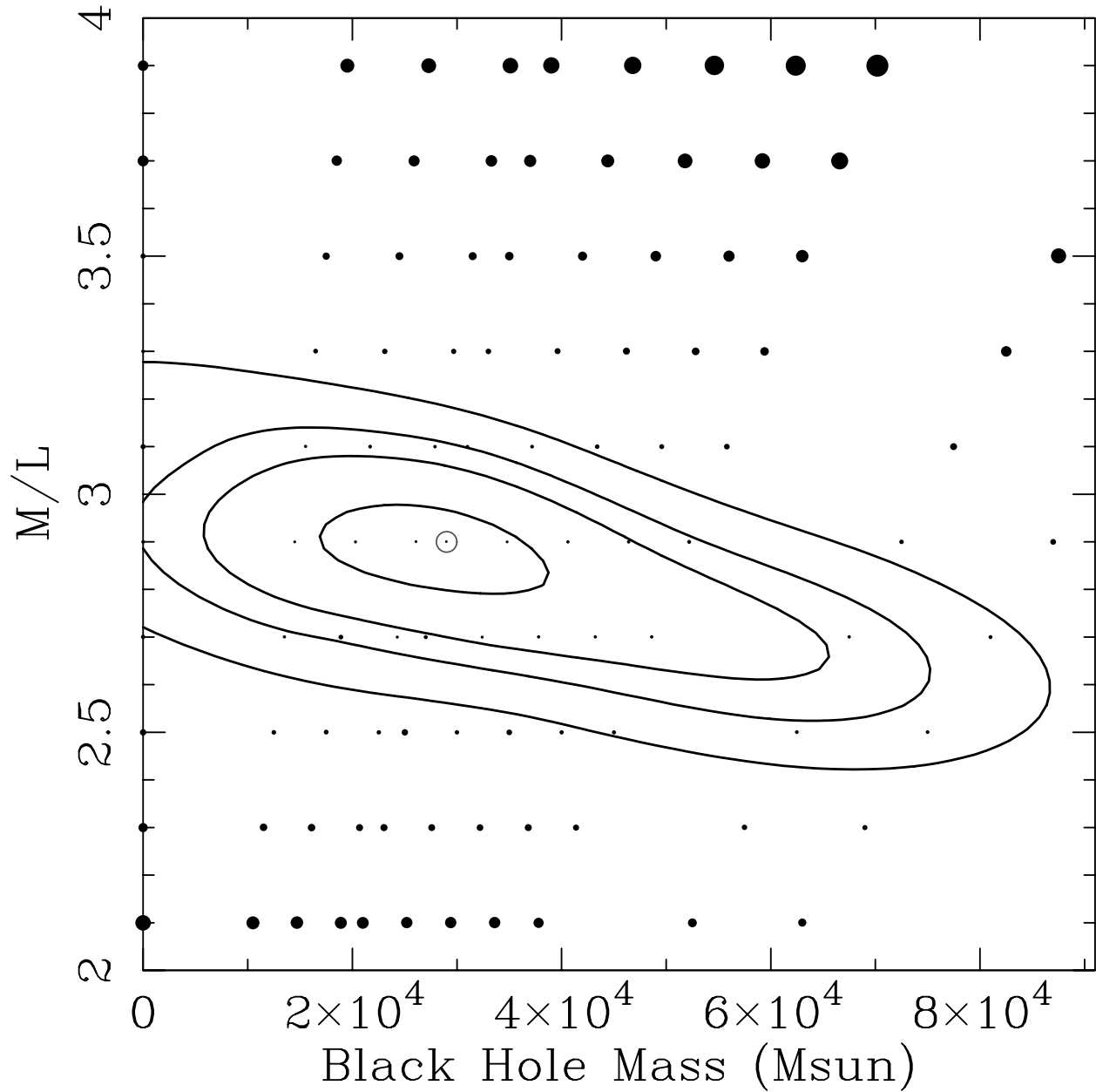
Fig. 7.— Contours of χ^2 as a function of black hole mass and mass-to-light ratio. Each point represents a particular model. The contours represent the 68, 90, 95, and 99% confidence for one degree-of-freedom, implying $\Delta\chi^2 = 1.0, 2.7, 4.0$, and 6.6. The circled point is the model that has the minimum value.
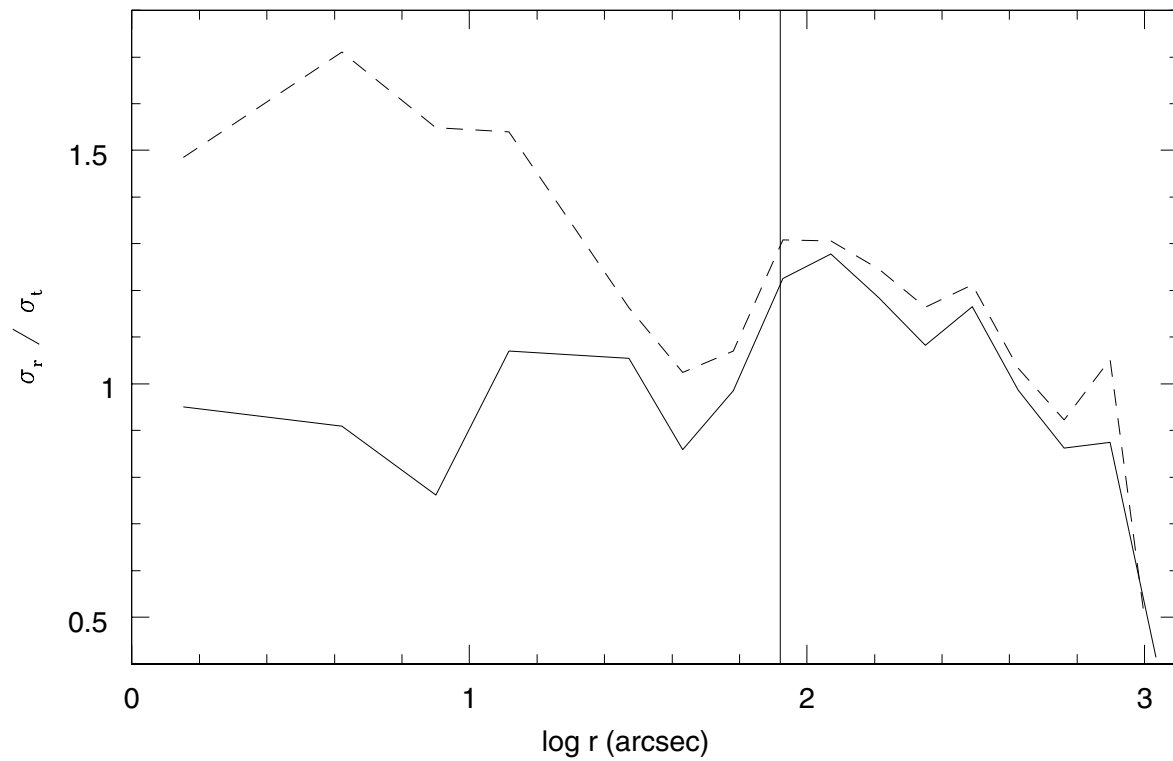
Fig. 8.— Radial over tangential anisotropy vs. radius from orbit-based models. The solid line is for the best fit model containing a black hole. Te dashed line is for a model with no black hole present. The vertical line marks the location of the core radius.
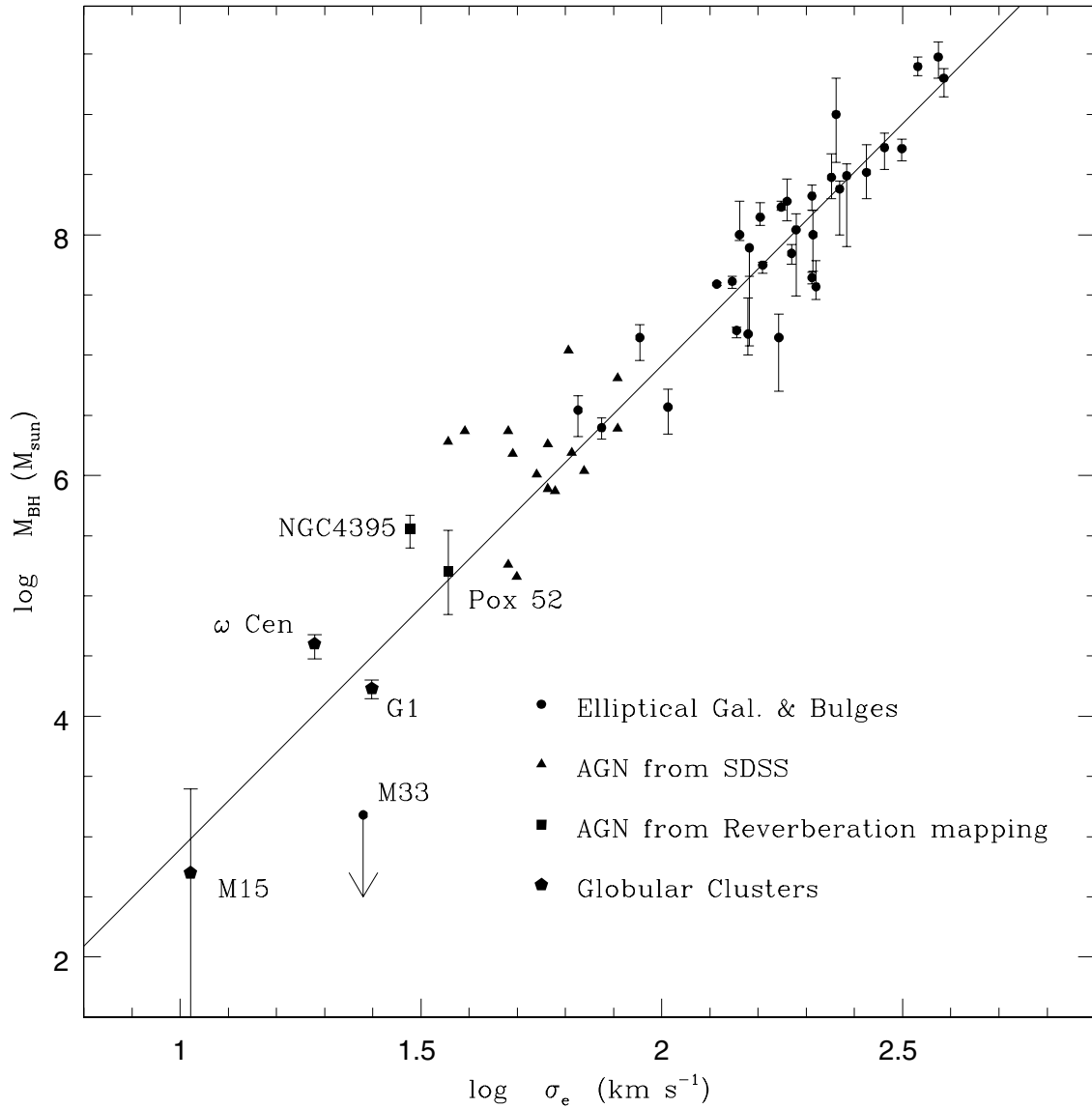
Fig. 9.— $M_\bullet - \sigma_{vel}$ relation for elliptical galaxies and bulges. The solid line is the relation in Tremaine et al. (2002). ω Cen lies on the low mass extrapolation and suggests a similarity between it and the galaxies. Different types of systems such as star clusters and low luminosity AGN appear to populate the low mass end of the diagram.